SpaceExpress: a method for comparative spatial transcriptomics based on intrinsic coordinate systems of tissues

Yeojin Kim[1], Abhishek Ojha[1], Alex Schrader[2], Juyeon Lee[2,3], Zijun Wu[1], Ian M Traniello[4], Gene E Robinson[5], Hee Sun Han[2,5*], Sihai D Zhao[5,6*], Saurabh Sinha[1,7*].

1 The Wallace H. Coulter Department of Biomedical Engineering, Georgia Institute of Technology, Atlanta, GA, 30332, USA
2 Department of Chemistry, University of Illinois Urbana-Champaign, Urbana, IL, 61801, USA
3 School of Biological and Environmental Studies, Millikin University, Decatur, IL 62522, USA
4 Lewis-Sigler Institute for Integrative Genomics, Princeton University, Princeton, NJ, 08544, USA
5 Carl R. Woese Institute for Genomic Biology, University of Illinois Urbana-Champaign, Urbana, IL, 61801, USA
6 Department of Statistics, University of Illinois Urbana-Champaign, Urbana, IL, 61820, USA
7 H. Milton Stewart School of Industrial & Systems Engineering, Georgia Institute of Technology, Atlanta, GA, 30318, USA

* Corresponding Authors
Corresponding Authors-
1. Saurabh Sinha, Email- saurabh.sinha@bme.gatech.edu
2. Sihai Dave Zhao, Email- sdzhao@illinois.edu
3. Hee-Sun Han, Email- hshan@illinois.edu

ABSTRACT

Spatial transcriptomics (ST) technologies have enabled new explorations into the spatial organization of tissues and their functional implications. However, one of the most fundamental analyses – comparative analysis of spatial gene expression across phenotypes – remains a formidable challenge. We introduce SpaceExpress, a novel statistical tool for detecting phenotype-associated changes in spatial expression patterns. SpaceExpress employs a neural network to embed multiple ST samples in a common latent space, enabling robust cross-sample comparisons despite structural and technical variations. It then uses spline regression to test differential spatial expression of genes between conditions, with rigorous false discovery control and handling of multiple replicates per condition. It includes visualization tools to help interpret spatial pattern differences. We demonstrate the tool's effectiveness on synthetic and real ST datasets, revealing mechanistic insights into behavior-related neurogenomic changes in honey bees and mice. Our work extends the highly influential paradigm of differential gene expression analysis to spatial omics.

INTRODUCTION

The rapid development of highly multiplexed spatially resolved omics technologies, including spatial transcriptomics (ST)[1, 2], has opened new avenues of inquiry into the interplay of intercellular communication and intracellular gene regulatory mechanisms, as well as the spatio-temporal organization of tissues and its relationship to function. Concurrently, analysis tools have been developed for detection of spatially varying genes[3, 4], spatial domains[5], and cell-cell communication[6, 7] for ST data. As ST technologies mature and costs decrease, research groups will be able to collect ST measurements from many samples to understand how the fine global structure of spatial gene expression might be associated with phenotypes such as disease states and quantitative traits. This type of comparative analysis will be an important step in advancing from the largely descriptive nature of current ST analytics towards more mechanistic understanding of how biological systems function. To realize this goal, the field needs analysis tools that can quantify these associations in an interpretable way, as well as test for their statistical significance. For non-spatial transcriptomics data, rigorous detection of differential[8] or trait-associated[9] gene expression has been central to mechanistic studies. To the best of our knowledge, no such tools currently exist for spatial gene expression, posing a significant barrier to achieving the full potential of ST technologies.

This is a challenging problem for both technical and conceptual reasons. Technically, ST samples can vary for reasons that are not of direct interest, e.g., natural variation in tissue structure or differences in sectioning. Conceptually, it is difficult to even define a quantitative construct that can flexibly describe the innumerable ways in which the spatial structure of gene expression may associate with other traits. Available methods for describing spatial gene expression patterns in a tissue[10] do not furnish a way to compare those patterns across tissues, especially in the face of structural variations noted above. Tools exist to align multiple ST samples[11, 12] or map cells across samples[13, 14] but these also do not provide a rigorous way to quantify associations between spatial expression patterns and traits.

We propose a novel approach to comparative analysis for spatial biology and use it to develop a statistical tool for inferring cross-sample or phenotype-associated changes in spatial expression patterns. Two key ideas underlie our solution. First, we observe that gene expression space can provide a common coordinate system that allows tissue structure to be compared across samples. This is based on the insight that a cell's expression profile encodes its spatial location, as explored by the positional information theory of spatial patterning[15]. We show that this common coordinate system can be learnt from ST data and allows for robust comparison across multiple samples despite structural variation. The second key idea is to represent cell locations using a coordinate-free nearest-neighbor graph and then embedding the cells into a latent Euclidean space. Each latent dimension represents a prominent spatial pattern present across the samples. These dimensions can be easily visualized and interpreted, and form the common coordinate system at the heart of our approach.

Our new tool, called SpaceExpress, learns a common coordinate system to describe spatial locations in given ST samples and uses these coordinates to rigorously test if a gene's spatial expression pattern changes across samples. The first step trains a neural network, constant across samples, that maps a cell's transcriptome to a low-dimensional representation (called the cell's "embedding") that reflects its spatial location relative to other cells. We demonstrate the superior accuracy of this representation through extensive evaluations on synthetic data and four different ST datasets obtained by three different technologies and comparisons with three state-of-the-art ST cell embedding methods[5, 16, 17]. We show that the learnt coordinate system represents underlying spatial biology of a tissue and is *shared* across analyzed samples, in the sense that biologically analogous regions of different samples are assigned similar coordinates, even for samples not seen during training. Included visualization tools aid in interpreting the coordinate system.

The second step of SpaceExpress uses the learnt shared coordinate system to directly compare spatial gene expression patterns between ST samples from different conditions. It employs spline regression modeling to formulate a rigorous hypothesis testing framework for differential spatial expression (DSE), thereby extending the widely popular paradigm of differential gene expression analysis[18] to the spatial omics domain. We use it to compare whole brain sections and specific brain substructures between a forager and soldier honey bee, using ST data that we generated, and identify statistically significant DSE genes that yield mechanistic hypotheses about behavior-related neurogenomic changes. We also use SpaceExpress to compare two groups of ST samples from the mouse hypothalamic preoptic area, highlighting spatial expression differences associated with aggressive behavior. In summary, we present a novel approach to multi-sample ST data analysis capable of identifying spatial axes capturing the fine global structure shared by those samples, and rigorously testing the differential spatial expression of genes.

RESULTS

Overview of SpaceExpress

SpaceExpress is the first approach that can rigorously test whether a gene's spatial expression pattern differs between samples. More generally, it can test if spatial differences in gene expression are associated with a trait across multiple spatial samples. Furthermore, it can characterize these associations in a way that aligns with the tissue's inherent biological organization. It is challenging to compare expression patterns along conventional x-, y-, and z-axes, since the correspondence between standard Cartesian coordinates and biologically relevant spatial features – such as developmental axes or tissue layers – varies across samples. SpaceExpress overcomes this fundamental limitation by learning latent dimensions that reflect the tissue's intrinsic biological organization, enabling more meaningful comparisons of spatial gene expression patterns.

SpaceExpress first constructs a coordinate-free representation of each sample using a nearest neighbor graph of its cells, then learns a *d*-dimensional vector representation, called an "embedding", of each cell such that a pair of cells close (resp. far) in a sample's graph have similar (resp. different) embeddings (**Figure 1**, Methods). The dimensionality *d* is user-configurable. Next, it trains a neural network to learn a cell's embedding as a function of its gene expression profile. This is motivated by the insight that gene expression encodes spatial location, arising from the literature on "positional information"[15]. The embedding dimensions can be viewed as defining an intrinsic coordinate system that captures the fine global structure of the tissue as encoded in its transcriptome. Since gene expression, when properly normalized, is comparable across samples, the embeddings are automatically comparable as well. The dimensions are invariant to technical variation such as rotation or scaling, adapt to complex tissue geometries, and can be easily interpreted by visualizing the embedding values of each cell in a tissue sample.

SpaceExpress uses the newly learned axes of spatial variation to characterize whether and how a gene is differentially spatially expressed with respect to discrete or quantitative traits. For this, it projects all cells onto each embedding dimension and models a gene's expression pattern as a mathematical function of the dimension. A gene is defined as differentially spatially expressed (DSE) with respect to a trait if this function varies across samples with different trait values (**Figure 1A,B**, Methods). Such an association is assessed in a statistical hypothesis testing framework. Differences in mean expression between samples are already accounted for in the model design, ensuring that they do not confound the identification of DSE. It is possible for a gene to be DSE for some dimensions but not others. This is a major advantage of SpaceExpress: it can identify which intrinsic tissue structures are involved in a gene's DSE.

SpaceExpress embeddings accurately capture space in synthetic and real data sets

The first step of SpaceExpress is to embed cells of the given ST sample(s) in a new, intrinsic coordinate system. We evaluated the extent to which these embeddings can accurately capture the relationship between expression and location in synthetic ST datasets. We synthesized an

"early *Drosophila* embryo slice" with cells laid out uniformly in an elliptical area, with a subset of genes varying in expression along the longer ("anterior-posterior" or "AP") axis and/or shorter ("dorso-ventral" or "DV") axis (**Figure 1C**, **Supplementary Table S1**). We used SpaceExpress to map each cell to a 4-dimensional embedding vector. To assess the accuracy of these embeddings, we calculated the Jaccard Similarity (JS) score between the nearest neighbor graph of cells based on their Cartesian coordinates (the "x-knn" graph) and their embeddings (the "p-knn" graph) (**Figure 1D**, Methods). We observed the JS score (theoretical range of 0-1) to be 0.45 on average (**Figure 1E**), significantly greater than the random expectation of 0.001 as well as that of state-of-the-art ST cell embedding approaches like STAGATE, SEDR and GraphST (**Figure 1E**). A Principal Components Analysis (PCA) visualization of the cell embeddings (**Figure 1F, Supplementary Figure S1**) and visualizations of the learnt dimensions using colormaps (**Figure 1G, Supplementary Figure S2**) provide further evidence that our embeddings accurately capture the AP and DV axes and thus learn the intrinsic coordinate system of this data set.

A tissue's spatial organization often comprises a set of discrete spatial domains or regions[5]. To test our model's ability to capture this type of organization, we synthesized a "domain grid" ST data set with nine different spatial domains arranged in a square grid (**Figure 1H**), each domain distinguished by a marker gene's expression **(**Methods**)**. SpaceExpress embeddings (JS score of 0.8 on average) were substantially more accurate than other methods (**Figure 1I,J, Supplementary Figure S3**). We also assessed the extent to which SpaceExpress embeddings capture expression (**Supplementary Figure S4**) and observed that, compared to other embedding methods, they reflect spatial proximity more strongly than expression similarity. This underscores the different trade-offs made by different cell embedding methods when integrating expression and spatial information.

We next undertook similar assessments on real ST datasets obtained using different technologies. Our first evaluation was on the commonly analyzed dorsolateral pre-frontal cortex (DLPFC) data obtained by Maynard et al.[19] using 10X Visium technology. We analyzed 12 different samples (from 3 different donors) separately, and observed significantly higher JS scores for SpaceExpress embeddings than STAGATE, SEDR, and GraphST (**Figure 2A, Supplementary Data S1**). In all samples, one of the learnt dimensions captures a transverse axis through the cortex layers**,** despite substantial differences in tissue spatial structure (**Figures 2B,C**, **Supplementary Figure S5)**. In an additional evaluation motivated by the layered structure of these tissue samples, we validated that (a) cells in more spatially separated layers are embedded more distally to each other than cells in proximal layers, and (b) cells in the same layer are embedded more proximally to each other if they are located nearby in physical space; in both regards SpaceExpress is competitive with or better than other methods (e.g., see **Supplementary Figure S6, Figure 2D** for results on sample ID 151507). We also evaluated the tool's embedding step on 16 samples of Drosophila late stage embryo (E14-16) profiled via STEREO-seq technology (Wang et al.[20]). Once again we noted significantly higher JS scores than those of other methods (**Figure 2E**) and a clear ability to capture the spatial organization of different regions in the embryo (**Figure 2F,G**). In summary, the evaluations reported here confirmed the ability of SpaceExpress embeddings to capture the spatial location of cells based on their transcriptome, across a variety of ST data sets.

SpaceExpress embeddings form a shared coordinate system across multiple samples

The intrinsic coordinate system learnt by SpaceExpress is capable of describing cellular locations across multiple spatial tissue samples. To demonstrate this ability, we first show that an embedding function trained on one tissue sample can predict spatial location from expression in an unseen tissue of a similar type. Specifically, we trained SpaceExpress embedding functions on a DLPFC sample (ID 151507) (Figure 2B) and used the trained model to embed cells of a different ("test") sample from another donor (**Supplementary Figure S7)**, without utilizing spatial information about them. We found these embeddings to successfully capture separations between layers (**Figure 3A**) as well as intra-layer distances between cells (**Figure 3A**) in the test sample. A visualization of the embedding dimensions for the test sample **(Supplementary Figure S8**) shows that they represent spatial directions analogous to those in the training sample. (See **Supplementary Figure S9** for additional tests.) The ability of SpaceExpress embeddings to capture spatial organization of the test sample is superior to that of an advanced spatial reconstruction tool called TANGRAM[13] (**Figure 3B**). We conducted similar tests using the Drosophila embryogenesis data set, training SpaceExpress on the central slice, S08 (**Figure 2F**), and using it to assign spatial embeddings to other slices (**Figures 3C,D**) without accessing spatial information from the test slice. As shown in **Figure 3E** and **Supplementary Figures S10**, the spatial organization of cell types in these embryonic slices is well captured by the SpaceExpress embeddings. These tests demonstrate that the SpaceExpress cell embedding model captures space in a way that transcends the specific spatial coordinate system and cellular arrangements of the given tissue and is relevant even for other specimens of the tissue type. We note that no existing tool is capable of such generalizability: current ST embedding tools[5, 16, 17] require spatial location information to embed cells, while tools like TANGRAM[13] are intended to *map* a non-spatial scRNA-seq sample onto a reference spatial sample.

Our next tests show that when SpaceExpress analyzes two or more ST samples, the embedding dimensions learnt by it establish a "universal" coordinate system where biologically similar regions in different samples, e.g., functional domains, positions on a biological axis, etc., are assigned similar coordinates. First, we generated two synthetic "early embryos" (Figure 1E) using the same rules of spatial expression variation as above (Supplementary Table S1), but also introduced inter-embryo differences in spatial patterns of a subset (20%) of genes (**Figure 3F**, Methods, **Supplementary Figure S11**). We trained SpaceExpress on the two embryos jointly to obtain a 4-dimensional coordinate system and used the predefined correspondence between cells in the two embryos to calculate the agreement (between embryos) of SpaceExpress-assigned coordinate values, for each learnt dimension separately. The agreement, computed as the slope of a best-fit line relating the coordinates in the two embryos, is approximately equal to 1 **(Figure 3G,H**, **Supplementary Data S2**), indicating that SpaceExpress accurately learns a shared coordinate system. We performed similar tests with the Drosophila embryogenesis STEREO-seq data, where a cell-to-cell mapping between adjacent pairs of slices is available[20]. Using SpaceExpress to jointly analyze slice S8 and one of its adjacent slices (S07 or S09), we found the learnt dimensions to be in high agreement (slope = 1.027-1.028), as is visually supported by **Supplementary Figure S12**.

In summary, the above evaluations of multi-sample analysis find the first step of SpaceExpress to reveal a biologically meaningful, intrinsic coordinate system for a tissue, allowing its second step to perform a robust comparison of spatial expression patterns across different samples.

SpaceExpress identifies and characterizes differentially spatially expressed genes

The second step of SpaceExpress involves a rigorous statistical inference procedure for differential spatial expression (DSE), achieved via nonparametric regression modeling (**Supplementary Figure S13**, Methods). Once cells of all tissue samples have been embedded in a common d-dimensional space, each gene is tested for DSE along each of the dimensions, with false discovery rate (FDR) control. This involves fitting a spline regression model of a gene's expression in a cell and using likelihood ratio statistics to assess if the contribution of the cell's coordinate value to the model is sample-specific (or in the case of more than two samples, group-specific). FDR control is achieved using an empirical null fitting procedure[21]. The first step of learning a shared coordinate system is prone to being compromised by DSE genes, since such genes, by definition, violate the premise of gene expression encoding space in a "universal" manner. To address this, once DSE genes have been identified, the embedding functions are retrained without using those genes, and the statistical testing procedure is repeated a second time. We justify the individual steps of our testing procedure through **Supplementary Data S3**.

We performed systematic tests of the sensitivity and precision of our approach using the simulated pairs of "early embryos", where 20 of 100 genes are made DSE in a controlled manner (Methods). Figure 3F illustrates a gene with a moderate level of DSE manifested along the AP as well as DV axis (**Supplementary Figure S14A,B**), and we saw above that SpaceExpress captures their AP and DV axes automatically (**Figure 3H**, **Supplementary Figure S15**). **Figure 3I** shows the gene's expression in individual cells plotted against the cell's coordinate in dimension 1, with the spline regression model fit to these data, revealing the separate trends of expression versus embedding dimension in the two embryos. This divergence is quantified in a high log likelihood ratio statistic, which is then assigned an FDR of approximately 0. As shown in **Supplementary Data S3** (row $\mu = 0.6$), the pipeline identifies all 20 DSE genes as significant (FDR $\leq$ 0.001), with 2 false positives (out of the 80 non-DSE genes). Similarly high sensitivity and precision were noted even for small values of μ (Supplementary Data S3), representing fine changes in spatial expression that are difficult to detect visually (**Supplementary Figure S14C,D**). In many cases the DSE was detected for the same gene in multiple embedding dimensions (**Supplementary Data S4**). Additionally, as shown in **Supplementary Figure S16**, SpaceExpress can detect DSE genes that are not identified by traditional differential expression (DE) analysis.

SpaceExpress pinpoints behavior-related changes in the honey bee brain spatial transcriptome

We illustrate the power of SpaceExpress by using it to identify DSE patterns associated with honey bee behavior. Honey bees form complex societies with specific castes responsible for different tasks and previous research has revealed that neurotranscriptomic state is tightly linked

to a bee's occupation in the hive[22-24]. However, these transcriptomic states[22, 23, 25, 26] have lacked spatial resolution and it remains unclear whether behavioral differences between castes such as soldiers and foragers are associated with regional variations in expression. Studying anatomical locations responsible for this DSE may reveal principles of how complex behaviors emerge from the spatial organization of cells in the bee brain.

To answer this question, we profiled the spatial expression of 130 behavior-related genes[25, 26] in similarly aged soldier and forager brains using our custom MERFISH platform and performed spatial comparisons using SpaceExpress. For the forager brain we intentionally used a section that was only partially imaged (**Figure 4A**), to mimic the common challenges for differential spatial analysis, including size/morphology variation and partially damaged tissues. **Figure 4B** visualizes a four-dimensional intrinsic coordinate system learned by SpaceExpress on the two brains. Despite dramatic visual differences between the samples, each learned dimension successfully captures anatomical structures previously characterized in honey bee brains, and assigns similar coordinates to the same regions across both brains. Additionally, different embedding dimensions distinguish different structures. For example, dimensions 2 and 4 clearly distinguish between mushroom bodies (MB), the primary region responsible for learning[27], and the rest of the brain. Dimension 1 differentiates regions within MB, which correspond to different subtypes of neurons called Kenyon cells (**Supplementary Figure S17**). Dimension 4 differentiates between the central complex (middle embedding values) and the optic lobes (low embedding values), which is especially noteworthy because the central complex was not even imaged in the forager brain sample.

Based on these embeddings, SpaceExpress found 27 unique DSE genes at an FDR of 0.005 across all four embedding dimensions (**Figure 4C**). Our spline model allows for different average expression levels (see **Methods**), ensuring that these findings were not driven by overall differential expression (DE) of a gene between the two samples. To confirm this, we tested for overall differential expression of each gene using a Wilcoxon test, and found DE and DSE ranks of genes to be uncorrelated (**Supplementary Figure S18**).

A unique advantage of the SpaceExpress framework is that its embedding visualizations can be used along with its fitted spline models to interpret DSE patterns and derive biological insight. For each DSE gene, SpaceExpress produces a consolidated report with figures showing the spatial expression patterns in the samples, visualizations of the embedding dimension in which the DSE was detected, and a plot of the best-fit spline models showing how expression varies with the embedding dimension in each sample. We highlight a few of our results below.

Some genes show a similar spatial expression pattern across an embedding dimension between the two phenotypes, except in a localized region. This is evident in the dimension 1 spline plots for *hr38* (DSE FDR 1.8×10^{-11}), where the expression in the soldier differs from the forager approximately between embedding values -7 and -4, where it shows a peak (**Figure 4E**). The embedding visualization of dimension 1 (Figure 4B) shows that these embedding values roughly correspond to the large Kenyon cells of the MB (Supplementary Figure S17), indicating that *hr38* is more spatially localized to these cells in the soldier than in the forager (**Figure 4D**). Corroborative of these findings, *in situ* hybridization has previously shown that spatial localization

of this immediate early gene within the MB varies with aggressive responsiveness in honey bees, though overall expression levels do not change across aggressive or affiliative contexts[28].

Some genes' spatial expression patterns look different across most of the embedding dimension. For example, the dimension 3 spline plots for *fasciclin-1* (DSE FDR 0.0) show that in the soldier, the gene has higher expression for embedding values in the range 3 – 5 (blue in Fig. 4B) compared to values around -3 (green in Fig. 4B), while this trend is absent for the forager (**Figure 4G**). Given the embedding visualization of dimension 3 (Figure 4B), this suggests that *fasciclin-1* is spatially more expressed near the optic lobes than large Kenyon cells of MB in the soldier, in contrast to the pattern in the forager (**Figure 4F**). Interestingly, *fasciclin-1* is associated with synaptic plasticity[29], which is important for behavioral differences.

We also found the circadian clock gene *per* to be DSE along dimension 4 (DSE FDR 2.6×10^{-4}), and the associated visualizations (**Figure 4B,H,I)** reveal that its expression is concentrated in the MB in both brains, but more so in the soldier. We anticipate substantial variation in timekeeping strategies between soldiers and foragers: foraging behavior is gated by diurnal nectar and pollen availability[30], whereas soldiers must always be prepared to launch an attack at the earliest indication of a threat. Therefore, variation in circadian-associated localization may indicate a mechanistic underpinning of phenotypic variation across soldiers and foragers.

SpaceExpress pinpoints behavior-related changes in the mouse hypothalamic preoptic area spatial transcriptome

We next applied SpaceExpress to identify genes whose spatial expression patterns in the hypothalamic preoptic area of virgin male mice differ based on pup-exposure, which is associated with aggressive behavior. We analyzed MERFISH data from one control and one pup-exposed mouse, collected by Moffitt et al.[31]. The four-dimensional intrinsic coordinate system learned by SpaceExpress (**Figure 5C**) captures meaningful tissue structure despite dramatic differences between the samples. Roughly, dimension 1 identifies the dorsal-ventral axis, dimension 2 highlights a gradient that increases from the medial preoptic area (MPA) and fornix (fx) to the periventricular zone (PV) and bed nucleus of the stria terminalis (BST), dimension 3 spans third ventricle (V3) and fx on one extreme and MPA on the other, while dimension 4 distinguishes the median preoptic nucleus (MPN) from the rest of the MPA. Importantly, these embeddings do not simply cluster known brain regions, they also identify continuous gradients within each region. For example, the dimension 3 embeddings exhibit a gradient within the V3 region. To support these embedding interpretations, we transferred expression-based brain region annotations from Li et al.[32] using the tool SLAT[12] (**Figure 5A,** Methods).

Based on these embeddings, SpaceExpress identified 41 unique DSE genes at an FDR of 0.005 (**Figure 5B**). These include the gene *Th* (tyrosine hydroxylase), which is DSE with FDR ~0 in dimension 3. **Figure 5D** and **Supplementary Figure S19** show that the contrast in *Th* expression between fx and V3 regions versus BST and MPN regions in stronger in the pup-exposed mouse compared to the naïve mouse. Th is crucial for neurotransmitter production, including dopamine and norepinephrine, which regulate emotional states including aggression[33, 34]. V3 surrounds key nuclei in the hypothalamus that regulate aggression[35] while fx is linked to emotional regulation

through connections to hypothalamus and hippocampus[36]. The fx- and V3-specific difference in *Th* expression thus suggests catecholamine signaling as a contributor to aggression toward pups[37]. A similar case of DSE is observed for the gene *Tac1*, which exhibits elevated expression in the V3 region, especially in the pup-exposed mouse **(Figure 5E, Supplementary Figure S20**): its expression along dimension 3 has opposing trends in the two samples (FDR ~ 0). *Tac1* encodes "substance P", a neuropeptide that is a key modulator of neurotransmission in regions involved in aggression such as V3[38], and our finding suggests that it may heighten aggression by amplifying the hypothalamic response to stressful stimuli such as pup-exposure. Many other genes well-known to be involved in aggression and parental behavior were also identified as DSE, including *oxytocin*[39, 40], *urocortin-3*[41], and *galanin*[42] (**Supplementary Figure S21**).

SpaceExpress can compare multiple biological replicates from different phenotype groups

A common paradigm in transcriptomics is to identify molecular changes, e.g., DE genes, between two groups of replicates representing different biological conditions or treatments[8]. SpaceExpress is the first tool to extend this influential paradigm to spatial transcriptomics in a statistically rigorous manner. The main idea is to include random effects terms into the SpaceExpress spline regression model (Methods).

We applied SpaceExpress to find DSE genes across three control mice and three pup-exposed mice collected by Moffitt et al.[31]. Here, we included cell type as an additional covariate of the model, to account for the potential confounding effect that varying cell types may have on spatial expression patterns (Methods). **Supplementary Figure S22** visualizes the common four-dimensional intrinsic coordinate system learned by SpaceExpress. We found 19 DSE genes at an FDR of 0.001, including well-known genes such as *oxytocin* and *urocortin-3*. (The FDR threshold here is higher than above because of the much smaller sample size – number of replicates rather than number of cells.) For instance, the *Oxt* (oxytocin) gene is DSE in dimension 4 (FDR ~ 0), with the two groups of replicates diverging in their expression levels for embedding values greater than 0 (**Figure 6A**). This roughly corresponds to the BST and PVH regions, as seen in **Supplementary Figure S22** and **Supplementary Figure S23**, with the pup-exposed mouse brains exhibiting lower *Oxt* expression than naïve mice. This is consistent with recent work demonstrating that oxytocin activation in the PVH region inhibits pup-directed aggression[39] and with the known role of the BST region in such behavior[43].

In addition, our multi-replicate analysis found several genes that were not DSE in the previous no-replicate analysis, e.g., Gad1 (FDR 2e-4) in dimension 1. Visualizations of spline plots (**Figure 6B**) and the embedding dimension (**Supplementary Figure S22**) show that in pup-exposed mice *Gad1* expression drops and then rises between embedding values of -5 and 0, indicating that *Gad1* is high in the V3 and PV, high in the VLPO, and lower as cells get further from these two structures. In naïve mice *Gad1* rises continuously between embedding values -5 and 0 before also dropping at 0. Gad1 is a glutamate decarboxylase involved in synthesizing the inhibitory neurotransmitter GABA[44], suggesting that differing levels of inhibitory circuit activity in the regions around the VLPO may be related to pup-directed aggression. This finding is not visually obvious and requires all three replicates in each group, highlighting the unique advantages of an

interpretable quantitative framework for capturing and summarizing differential spatial expression across multiple biological replicates.

DISCUSSION

SpaceExpress enables the identification and biological interpretation of genes whose spatial expression patterns correlate with phenotypic traits. SpaceExpress can compare the spatial structure of gene expression across samples of highly organized tissue at the high spatial resolutions encoded in the tissue's transcriptome. This contrasts with existing tools that operate at coarser resolutions such as spatial domains[45], which can be used to identify differential gene expression in specific spatial domains across tissues[46-48]. It also differs from tools that study local spatial contexts, such as spatial "niches"[49] and "microenvironments"[50], which are more suitable for comparing tissues such as tumor samples.

A possible alternative to SpaceExpress is to align tissue samples and compare gene expression between aligned cells. However, this strategy faces technical challenges posed by structural variations across tissue samples, which makes alignment difficult[51], and it is hard to scale beyond pairwise comparisons (e.g., handling replicates) without treating one sample as a reference[52]. Our approach of leveraging positional information encoded in gene expression offers a more robust solution. Furthermore, it has the added advantage that we can visualize embedding dimensions and thus interpret the statistically detected DSE.

SpaceExpress, like other ST analysis tools, combines transcriptomic and spatial information to obtain low-dimensional embeddings of cells. A unique property of these embeddings is that the expression vector fully determines the embedding. This property enables the tool to embed cells profiled in non-spatial single-cell experiments as well. It can thus be used for "spatial reconstruction"[13, 14] without explicitly mapping to an arbitrary reference sample as is done today. The ability to generalize to unseen spatial data is also key to the model's robustness for learning intrinsic coordinate systems (**Supplementary Figure S24**).

The statistical methodology of DSE detection in SpaceExpress is capable of associating spatial expression patterns with quantitative as well as discrete traits. We have described results for binary traits but the underlying statistical framework allows quantitative traits to be accommodated as well. The model is highly flexible and can optionally accommodate cell type information through additional terms in the model (Methods)[48].

An important direction of future research is to systematically explore model complexity via tuning of hyperparameters, including the number of dimensions of the embedding space. Though the embedding space is meant to capture space (typically two- or three-dimensional), there can be value to using more than two embedding dimensions as each such dimension is meant to capture a biologically meaningful spatial pattern and there may be more than two such patterns, just as how the intrinsic dimension of a network object can be arbitrarily large.

METHODS

SpaceExpress Embeddings

The first step of SpaceExpress is to represent cells in a spatial transcriptomic (ST) dataset as low-dimensional vectors ("embedding" vectors or "embeddings"). Formally speaking, let the ST data set comprise a collection of cells C with each cell $c \in C$ being described by a gene expression vector $g(c)$ (of dimensionality G = number of genes) and a spatial location vector $x(c)$ of dimensionality two or three. Thus, the data set may be denoted by $D_{ST} = \{c, g(c), x(c)\}_{c \in C}$. Given D_{ST} and an integer d, the dimensionality of desired embedding vectors, SpaceExpress learns a function $F: \mathbb{R}^G \rightarrow \mathbb{R}^d$ that can map any given gene expression vector $g(c)$ to its d-dimensional embedding $p(c)$ such that for any two cells c_i, c_j in D_{ST}, the Euclidean distance between $p(c_i)$ and $p(c_j)$ reflects the spatial proximity between c_i and c_j. In this sense, the embedding function $F(g(c))$ is said to "capture space".

To make the previous definition precise, consider a k-nearest neighbor ("knn") graph whose nodes are all cells $c \in C$, and a directed edge from c_i to c_j is included if and only if cell c_j is among the k nearest neighbors of cell c_i based on their physical locations x. Here, k is a hyperparameter of the method, which is chosen as the smallest integer for which the graph is a connected graph, i.e., there is a path from every node to every other node. We now define the distance d_{ij} between any two cells c_i and c_j as the shortest path distance between their corresponding nodes in the knn graph. The function F introduced above is learnt so as to minimize the loss function $L = \sum_{c_i \in C, c_j \in C, i \neq j} \frac{1}{d_{ij}^2} \left(\left\| p(c_i) - p(c_j) \right\| - d_{ij} \right)^2$, where $p(c) = F(g(c))$ and $\|\cdot\|$ represents the L_2-norm of a vector. This loss function, henceforth called "KK" loss, is a special form of the Kamada-Kawai loss function used in network layout applications[53]. It is a sum over all pairs of cells (c_i, c_j) of the squared difference between d_{ij} (their spatial distance, as defined above) and $\left\| p(c_i) - p(c_j) \right\|$ (Euclidean distance between their embedding vectors), but with each term being weighted by $\frac{1}{d_{ij}^2}$, thus down-weighting errors made on more distant pairs of cells. The training of function F, also called the "model", can be done on one ST data set, as explained above, or on multiple data sets; in the latter case, the loss function used is the sum over the KK loss on each data set. Once trained, the model may be used to map the cells of any new data set, using only their expression vectors $g(c)$, to their corresponding embeddings $p(c)$, without requiring their spatial locations. SpaceExpress determines the optimal value of k by iteratively increasing k from 4 to 20 and selecting the smallest k that results in a fully connected graph. If no such k is found within this range, it first generates a graph with the smallest k that minimizes the number of connected components, then connects the physically closest pairs of nodes from different components to achieve full connectivity. Specifically, for n disconnected components, it adds n−1 edges to connect them: It finds the closest cell pair straddling two disconnected components and connects them with an added edge, repeating this process until all components are mutually connected.

When training on multiple ST datasets, SpaceExpress performs joint training to learn a shared embedding function F that captures spatial relationships across all datasets. Suppose we

have n datasets. For each dataset, the same number of cell pairs are randomly selected to ensure equal contribution from each dataset. The KK loss is computed separately for each dataset, resulting in individual losses L_i for $i = 1,2, \ldots, n$. The total loss function used for training is the sum of the individual losses: $L = \sum_{i=1}^{n} L_i$. This approach allows the model to generalize across different samples and conditions, effectively integrating multiple datasets into a unified embedding space. In the implementation, during each training epoch, a fixed number of cell pairs from each dataset are randomly sampled to compute the KK loss to prevents the model from being biased toward larger datasets.

The function F that generates $p(c) = F\big(g(c)\big)$ is a neural network with an input layer comprising G neurons (one for each gene's expression value), an output layer with d neurons and a single hidden layer with h neurons (h is a hyperparameter), and two fully connected layers, for a total of $O(Gh + dh)$ free parameters. Parameter optimization is implemented using Adam optimizer. The full collection of $\binom{|C|}{2}$ cell pairs is partitioned at random into N_{mb} equal subsets and these subsets are used as mini-batches in each epoch. Batch normalization is used as a form of regularization, and though we explored the use of dropouts and L1/L2 regularization these features were not used in the final implementation as they did not yield significant improvement on unseen data.

Preprocessing: Each dataset was preprocessed by filtering out genes expressed in fewer than 3 cells and cells expressing fewer than 3 genes. The data was normalized to a target sum of 10,000 (each cell by total counts over all genes) and log transformed. To minimize the influence of extreme values, gene expression values were capped at the 95th percentile. The user may optionally select to use either all genes or only the most highly variable genes (HVGs); the number of HVGs to use (n_{HVG}) is a configurable parameter. If the user selects to use HVG-based analysis, SpaceExpress identifies the n_{HVG} highest variance genes in each sample, calculates the intersection of these HVGs across all samples, and creates a limited version of each sample's data that includes only these genes, and scales each gene in each sample to unit variance and zero mean.

Synthetic data sets

"Early embryo slice" data set: Each such data set comprises 3,915 cells placed uniformly in an elliptical area whose major and minor axes, called "anterior-posterior" (AP) or "dorso-ventral" (DV) axes, have lengths of 100 and 50 units, respectively. The transcriptomic data synthesize spans 100 genes that fall into the following categories:

- AP genes (20): these include two "core" AP genes AP1 and AP2, whose expression in a cell with coordinates (x, y) is given by $e^{-\frac{x^2}{40^2}}$ and $e^{-\frac{(x-100)^2}{40^2}}$ respectively. Here, the major (AP) and minor (DV) axes defined the x and y coordinates of a cell, with x ranging from zero at the left (anterior) end of the major axis to one at the right (posterior) end, and y ranging from zero at the top (dorsal) end of the minor axis to one at the bottom (ventral) end. An additional 18 "derivative" AP genes are assigned expression values according to the formula $\alpha_i \cdot AP_1 + (1 - \alpha_i) \cdot AP_2$ i.e., a weighted combination of AP1 and AP2 expression profiles. Each derivative

gene uses a weight α_i chosen at random from the range $[0,1)$. Note that all 20 AP genes have an "AP" expression pattern, i.e., the expression is identical in all cells at a fixed x coordinate (position along the AP axis).

- DV genes (20): these are assigned expression patterns similarly to the AP genes except that their expression varies along the DV axis and all cells with the same y coordinate have the same expression value for a DV gene. There are two core DV genes – DV1 and DV2 – with expression values given by $e^{-\frac{y^2}{20^2}}$ and $e^{-\frac{(y-50)^2}{20^2}}$ respectively, and 18 derivative DV genes whose expression is a weighted combination of DV1 and DV2.
- APDV genes (20): each such gene is defined by the formula $\frac{1}{2}(\gamma_{k0} \cdot AP_1 + (1-\gamma_{k0}) \cdot AP_2 + \gamma_{k1} \cdot DV_1 + (1-\gamma_{k1}) \cdot DV_2)$ for $\gamma_k \sim \mathrm{Unif}[0,1)$, i.e., sum of an AP and a DV expression pattern, each being a weighted sum of the respective core genes.
- Randomly expressed genes (40): For each of these genes, we assign an expression pattern in each cell independently at random in the range $[0,1]$. These genes have no spatial pattern.

Once each gene's expression level e is assigned in each cell, an expression "count" is sampled from the Poisson distribution with parameter $1000e$.

"Cluster" data set: Each such data set comprises 900 cells placed uniformly in a 30 x 30 grid, organized as 3 x 3 = 9 "regions" of 10 x 10 = 100 cells each (Figure). Each region is "marked" by a gene that is assigned an expression level of 1 in all 100 cells of that region and 0 in all remaining 800 cells. Thus, there are nine marker genes G1, G2, …, G9, corresponding to the nine regions respectively. An additional 91 genes are assigned random expression levels selected uniformly from $[0,1]$ independently for each cell. Once expression values have been assigned in this manner, an expression "count" is sampled from the Poisson distribution with parameter equal to 1000 times that assigned value.

Use of existing software

In this study, we utilized SEDR[16], GraphST[17], and STAGATE[5] as benchmark methods to compare their embeddings with SpaceExpress. For SEDR, during the preprocessing step, if a dataset contained fewer than 200 genes, we removed the PCA step used for dimensionality reduction to 200. For STAGATE, we set each spot or cell to have six neighboring cells, following the original paper's protocol. All other parameters were kept at their default settings as specified by the original authors. To map the locations of cells based solely on their transcriptomes, we used Tangram with default parameters. The DLPFC[19] dataset (ID 151507) was used as the spatial transcriptomic data, while a sample from another donor, with spatial information removed, was used as the single-cell dataset. For marker genes in Tangram, we selected the top 1,000 highly variable genes.

Evaluation of embeddings

To evaluate how well a given set of embeddings ($p(c)$ for all cells c in a data set) capture space, we construct a k-nearest neighbor graph based on the locations $x(c)$ of cells, called the "x-knn" graph, and a k-nearest neighbor graph based on the embeddings $p(c)$, called the "p-knn" graph. In both cases, Euclidean distances are used to find nearest neighbors. We then calculate the Jaccard similarity score JS(x-knn, p-knn) as $\frac{|E_x \cap E_p|}{|E_x \cup E_p|}$, where E_x and E_p are sets of edges (cell pairs) in the x-knn and p-knn respectively.

To evaluate how well embeddings capture gene expression, we adopt a similar procedure as above, now constructing a k-nearest neighbor graph based on the gene expression vectors $g(c)$ of cells ("g-knn" graph), but using cosine similarities instead of Euclidean distances to define nearest neighbors, on account of the high dimensionality of expression vectors. We then calculate the Jaccard similarity score JS(g-knn, p-knn) as $\frac{|E_g \cap E_p|}{|E_g \cup E_p|}$, where E_g is the set of edges (cell pairs) in the g-knn.

Real data sets

We utilized SpaceExpress to analyze spatial transcriptomic datasets generated by various platforms, including 10x Visium, Stereo-seq and MERFISH. The human dorsolateral prefrontal cortex (DLPFC) dataset, generated using the 10x Visium platform, includes 12 sections from three individuals[19]. This dataset contains 33,538 genes, with the number of spots per section ranging from 3,460 to 4,789. The Drosophila embryo dataset, generated using the Stereo-seq platform[20], includes 15 sections from the same embryo. For evaluation, we used five consecutive sections (IDs 6 to 10), with each section containing between 815 and 1,272 spots and 13,668 genes.

In the case study, we analyzed the mouse brain hypothalamic preoptic dataset[31], which consists of six samples, each with 4,908 to 5,998 cells and 155 genes. For 1:1 comparison between naïve and pup-exposed samples, we used one male naïve sample (ID 5) and one male pup-exposed sample (ID 36), both at bregma 0.16. For the analysis of multiple biological replicates from different phenotype groups, we selected male naïve samples (IDs 5, 6, 7) and male pup-exposed samples (IDs 34, 35, 36), all from the same bregma (0.16).

Synthetic data sets with differential spatial expression

To test the ability of SpaceExpress to learn "shared" coordinate systems, we synthesize a pair of "early embryo slice" data sets that are both organized using the AP and DV axes as coordinate axes, but exhibit a varying degree of divergence in that organization. Specifically, we follow the procedure outlined above to generate expression data for all but the "APDV" category of genes. Note that a gene in this category was assigned its expression value in a cell with coordinates (x, y) according to the formula $1/2(\gamma_{k0} \cdot AP_1 + (1-\gamma_{k0}) \cdot AP_2 + \gamma_{k1} \cdot DV_1 + (1-\gamma_{k1}) \cdot DV_2)$ where $\gamma_k \sim$ Unif$[0,1)$, i.e., a random combination of an AP pattern and a DV pattern. To

simulate differential spatial expression of these genes, we now modify this procedure as follows: in the first data set, we zero out the contribution of the AP pattern, so the new formula is $1/2(\gamma_{k1} \cdot DV_1 + (1-\gamma_{k1}) \cdot DV_2)$, meaning that such an "APDV" gene exhibits an exclusively DV pattern. In the second data set, we weight the AP pattern by a constant $\mu \in \{0.1, 0.2, \ldots 0.9\}$, so the new formula is $1/2((\mu \cdot AP_1) + (\gamma_{k1} \cdot DV_1 + (1-\gamma_{k1}) \cdot DV_2))$ and the "APDV" genes exhibit both a DV and an AP pattern with the strength of the latter being controlled by μ. All 20 APDV genes use the same value of μ in a data set. Thus, a pair of data sets comprises one embryo where APDV genes have zero AP pattern and one embryo where the AP pattern is weighted by a fixed value of μ. In this way we can generate pairs of data sets exhibiting varying degrees of DSE, by progressively increasing the value of μ.

Differential Spatial Expression analysis between two samples

Goal: In this section, we describe how SpaceExpress assesses differential spatial expression (DSE) of genes between two ST samples. We assume that the first step has learnt the shared coordinate system of the two samples, by embedding each cell in a latent Euclidean space. For each embedding dimension, SpaceExpress analyzes each gene separately and then combines the results via appropriate multiple-hypothesis testing procedure. As a result, we get a set of DSE genes for each embedding dimension.

Pre-processing: For a given gene, we log-transform the expression and then remove the cells that are beyond 4 standard deviations away from the mean. We drop a gene from the analysis if the transformed expression values are all zero in any group. We scale (without centering) the transformed expression within each group to have unit variance.

Linear Models: As mentioned in the goal, the analysis involves regressing each gene on each embedding dimension separately. For the sake of interpretation and statistical inference, we decided to use a linear model to fit gene expression against a given embedding dimension. However, a linear function of the embedding values will not be sufficient to capture the variation. Therefore, we use a spline regression strategy, where we create spline basis functions based on an embedding dimension. These spline basis functions are non-linear functions of the embedding dimension. Consequently, we can regress gene expression as a linear function of these spline basis functions. This approach allows us to retain the statistical interpretation advantages of a linear model while achieving a fit that is a non-linear function of the embedding. The generation of spline basis functions depends on a crucial parameter known as degrees of freedom. Higher degrees of freedom correspond to more non-linearity. We generate natural cubic spline bases with 300 degrees of freedom using the *ns* function from the *splines* package in R. For cell i, we denote the transformed and scaled gene expression by Y_i, the generated spline basis vector by X_i^d(d denotes the embedding dimension), and the group identity by G_i. We fit the following two linear models using the *lm* package in R:

$$Y_i = \alpha + \beta^T X_i^d + \gamma G_i + \delta^T\left(G_i X_i^d\right) + \epsilon_i \text{ (full model: with interaction term),}$$
$$Y_i = \alpha + \beta^T X_i^d + \gamma G_i + \epsilon_i \text{ (null model: without interaction term).}$$

Here ϵ_i are assumed to be independent Gaussian errors with zero mean. The interaction term δ represents the differential spatial expression between the two groups. Therefore, we test the significance of δ via a likelihood ratio test (LRT) between full and the null models. Furthermore, the γG_i term in the null model accounts for the mean expression difference between the two groups, ensuring that the observed effects are not simply due to overall differential expression (DE).

Multiple Hypothesis testing via Empirical Null method: For embedding dimension d , we collect the LRT based chi-squared test statistic for each gene. We estimate the empirical null distribution and then the false discovery rate (FDR) for each gene using the method described by Ren et al.[21]. As an implementation detail, the quantile parameter, q, for empirical null calculation that we use is 0.75.

Multi-replicate Differential Spatial Expression analysis

Goal: In this section, we describe how SpaceExpress assesses differential spatial expression (DSE) of genes across two groups with multiple replicates.

Pre-processing: For a given gene, we log-transform the expression and then remove the cells that are beyond 4 standard deviations away from the mean. We drop a gene from the analysis if the transformed expression values are all zero in any group. We scale (without centering) the transformed expression within each group. Furthermore, we generate natural cubic spline bases with 50 degrees of freedom using the *ns* function from the *splines* package in R.

Linear Mixed Effects Models: For cell i in replicate j we denote the transformed and scaled gene expression by Y_{ji}, the generated spline basis vector by X_{ji}^d (here d denotes the embedding dimension), the group identity by G_{ji}, and the cell type of cell i by C_i. We fit the following linear mixed effects model using *lmer* package in R:

$$Y_{ji} = \alpha + b_j + \beta^T X_{ji} + \gamma G_{ji} + \delta^T\left(X_{ji} G_{ji}\right) + \eta C_i + \epsilon_{ji} \text{ (full model: with interaction term),}$$
$$Y_{ji} = \alpha + b_j + \beta^T X_{ji} + \gamma G_{ji} + \eta C_i + \epsilon_{ji} \text{ (null model: without interaction term).}$$

Here b_j represents zero mean random intercept term. Other coefficients α, β, γ, δ, and η are assumed to be fixed effects across replicates. Furthermore, ϵ_{ji} are assumed to be independent Gaussian errors with zero mean. The interaction term $\delta^T\left(X_{ji} G_{ji}\right)$ represents the differential spatial expression between the two groups. Therefore, we test the significance of δ via a likelihood ratio test between full and the null models. We can drop the C_i term and the coefficient

η if we have just one cell type in the data or we do not want to capture the effect of cell types on the gene expression.

Multiple Hypothesis testing via Empirical Null method: For each embedding dimension, we collect the LRT based chi-squared test statistic for each gene. We estimate the empirical null distribution and then the false discovery rate (FDR) for each gene using the method described in Ren et al.[21]. As an implementation detail, the quantile parameter, q, for empirical null calculation that we use is 0.7.

MERFISH data generation for honey bee brain

MERFISH sample preparation: Honey bee MERFISH samples were prepared using a slightly modified published method[31]. Specifically, honey bee brains embedded in OCT were cryro-sectioned at a thickness of 5-7 µm. To reduce spot density, samples were embedded in an expandable poly-acrylamide gel using a previously published method[54].

MERFISH imaging: All images were acquired using a Zeiss Axiovert-200m widefield microscope (Carl Zeiss AG) located in the IGB core imaging facility. The sample was placed into a flow cell (Bioptechs, FCS2), filled with RNAse free 2x SSC, and connected to a lab built automated flow system. Briefly, computer-controlled valves (Hamilton, MVP/4, 8-5 valve) are used to select which solution was pulled across the sample by a computer controlled pump (Gilson, Minipuls 3). All systems are controlled by a custom designed Python script that can communicate with the microscope to start imaging or start flowing after an imaging round is done. In brief, a single round of imaging involves staining with fluorescently labeled readout probes (10% (v/v) ethylene carbonate (Sigma Aldrich), 0.1% Triton X-100 in 2x SSC, fluorescent DNA probe), washing with readout wash buffer (10% (v/v) ethylene carbonate, 0.1% Triton X-100 in 2x SSC) to remove unbound probes, and imaging buffer (5mM 3,4-dihydroxybenzoic acid (PCA; Sigma Aldrich), 2 mM trolox (Sigma Aldrich), 50 µM trolox quinone, 1:500 of recombinant protocatechuate 3,4-dioxygenase (rPCO; OYC Americas)), was flowed into the flow cell prior to imaging to reduce photobleaching. A single quad band excitation filter (Chroma, ZET402/468/555/638x) and dichroic (Chroma, ZT405/470/555/640rpc-UF1) were used to image all samples. Excitation was provided by a 7 laser system (LDI WF, 89 North). Alexa Fluor 647 (Fisher scientific) labeled probes were excited using a 647 nm laser (0.5 W) with a ET700/75m (Chroma) emission filter. Atto 565 (Atto tec) labeled probes were excited using a 555 nm laser (1 W) with an ET610/75m (Chroma) emission filter. Fiducial beads were imaged with a 405 nm laser (0.3 W) with a ET440/40m emission filter. Samples were imaged with a 63x oil immersion objective (Carl Zeiss AG, 420782-9900-000), and focus was maintained between imaging rounds using Definite Focus (Carl Zeiss AG). After imaging is complete, a cleavage buffer (0.05 M TCEP HCl, adjusted to a pH of 7-7.2 using 1 N NaOH, in 2x SSC) was flowed across the sample to remove the fluorophores from the probes. The cleavage buffer was washed away using RNAse free 2x SSC (0.5 mL/minute for 10 minutes). This process was repeated for a total of 8 rounds of imaging. PolyA probes were stained after the final imaging round using the same method as described above.

711 *MERFISH data processing:* Individual FOVs were exported from czi format into 16 bit tiff format
712 using Zen (Carl Zeiss AG) using the image export method. Images then were reformatted into
713 image stacks by FOV and round. A modified copy of MERLIN[55] was used to decode MERFISH
714 spots. In brief, for each FOV, images from different rounds are aligned using fiducial beads that
715 were imaged in each round. Aligned images are then normalized, decoded, and identified spots
716 filtered using previously published methods32. Cell segmentation was done separately from
717 MERLIN using Cellpose[56] on PolyA and DAPI images for each FOV. To improve FOV alignment
718 to neighboring FOVs, the DAPI channel was used with the restitching function found in Zen (Edge
719 detection: on, minimal overlap: 5%, maximal shift: 15%, comparer: best, Global optimizer: best).
720 Using the aligned images, segmented cells that cross FOV boundaries were merged into single
721 cells, and global positions were generated for each spot. Spots are then assigned to cells based
722 on their spatial coordinates. Spots were then filtered to remove any spot smaller than 3 pixels in
723 size.

724

725 **Obtaining neuroanatomical annotation of mouse brain**

726 We obtained the neuroanatomical annotations of the hypothalamic preoptic area in mouse brains
727 based on the manual annotations in Li et al.[32]. These annotations were made in tissue sections
728 at Bregma -0.14 mm from animal 1, and included eight domains (V3: third ventricle; BST: bed
729 nuclei of the stria terminalis; fx: columns of the fornix; MPA: medial preoptic area; MPN: medial
730 preoptic nucleus; PV: periventricular hypothalamic nucleus; PVH: paraventricular hypothalamic
731 nucleus; and PVT: paraventricular nucleus of the thalamus). We used this annotated section as
732 reference and aligned cells from sections of naïve mice (IDs 5, 6, 7) and pup-exposed mice (IDs
733 34, 35, 36) at bregma 0.16mm using SLAT[12] with default settings. The domains from the reference
734 cells were assigned to the mapped cells.

735

DATA AVAILABILITY

Dorsolateral Prefrontal Cortex (DLPFC) Dataset: The 10x Visium data used in this study is available at https://github.com/LieberInstitute/spatialLIBD.git[19]. Drosophila Late-Stage Embryo Dataset: Stereo-seq data can be accessed at https://db.cngb.org/stomics/flysta3d/[20]. Mouse Hypothalamic Preoptic Area Dataset: MERFISH data was obtained from[31], available at https://datadryad.org/stash/dataset/doi:10.5061/dryad.8t8s248. Honeybee Dataset: Data is available at https://doi.org/10.13012/B2IDB-5536668_V1.

CODE AVAILABILITY

SpaceExpress is implemented in Python, and the code is available at https://github.com/YeojinKim220/SpaceExpress. The package utilizes the AnnData format and can be installed by following the instructions on the GitHub page. A tutorial demonstrating SpaceExpress with data from the mouse hypothalamic preoptic region is also provided[31].

ACKNOWLEDGEMENTS

We thank Anurendra Kumar for valuable discussion. We thank Seokjin Yeo and Sunny Sun for image segmentation and Marisa Asadian for help for imaging. Funding: This work was supported by the National Institutes of Health (R35GM131819 to S.S., R35GM147420 to H.-S.H, R21HG013180 to S.D.Z. and H.-S.H.), and Georgia Institute of Technology (Wallace H. Coulter Distinguished Faculty Chair: S.S.) Facilities: We acknowledge Core Facilities at the Carl R. Woese Institute for Genomic Biology for their microscope and staff support.

REFERENCES

1. Rao, A., Barkley, D., França, G.S. & Yanai, I. Exploring tissue architecture using spatial transcriptomics. *Nature* **596**, 211-220 (2021).
2. Marx, V. Method of the Year: spatially resolved transcriptomics. *Nature Methods* **18**, 9-14 (2021).
3. Svensson, V., Teichmann, S.A. & Stegle, O. SpatialDE: identification of spatially variable genes. *Nature methods* **15**, 343-346 (2018).
4. Sun, S., Zhu, J. & Zhou, X. Statistical analysis of spatial expression patterns for spatially resolved transcriptomic studies. *Nature Methods* **17**, 193-200 (2020).
5. Dong, K. & Zhang, S. Deciphering spatial domains from spatially resolved transcriptomics with an adaptive graph attention auto-encoder. *Nature Communications* **13**, 1739 (2022).
6. Browaeys, R., Saelens, W. & Saeys, Y. NicheNet: modeling intercellular communication by linking ligands to target genes. *Nature Methods* **17**, 159-162 (2020).
7. Zhu, J. et al. Mapping cellular interactions from spatially resolved transcriptomics data. *Nature Methods* **21**, 1830-1842 (2024).
8. Squair, J.W. et al. Confronting false discoveries in single-cell differential expression. *Nature Communications* **12**, 5692 (2021).
9. Mancuso, N. et al. Integrating Gene Expression with Summary Association Statistics to Identify Genes Associated with 30 Complex Traits. *The American Journal of Human Genetics* **100**, 473-487 (2017).
10. Yuan, Z. et al. Benchmarking spatial clustering methods with spatially resolved transcriptomics data. *Nature Methods* **21**, 712-722 (2024).
11. Zeira, R., Land, M., Strzalkowski, A. & Raphael, B.J. Alignment and integration of spatial transcriptomics data. *Nature Methods* **19**, 567-575 (2022).
12. Xia, C.-R., Cao, Z.-J., Tu, X.-M. & Gao, G. Spatial-linked alignment tool (SLAT) for aligning heterogenous slices. *Nature Communications* **14**, 7236 (2023).
13. Biancalani, T. et al. Deep learning and alignment of spatially resolved single-cell transcriptomes with Tangram. *Nature Methods* **18**, 1352-1362 (2021).
14. Martin, P.C., Kim, H., Lövkvist, C., Hong, B.W. & Won, K.J. Vesalius: high-resolution in silico anatomization of spatial transcriptomic data using image analysis. *Molecular systems biology* **18**, e11080 (2022).
15. Dubuis, J.O., Tkačik, G., Wieschaus, E.F., Gregor, T. & Bialek, W. Positional information, in bits. *Proceedings of the National Academy of Sciences* **110**, 16301-16308 (2013).
16. Xu, H. et al. Unsupervised spatially embedded deep representation of spatial transcriptomics. *Genome Medicine* **16**, 12 (2024).
17. Long, Y. et al. Spatially informed clustering, integration, and deconvolution of spatial transcriptomics with GraphST. *Nature Communications* **14**, 1155 (2023).
18. Soneson, C. & Delorenzi, M. A comparison of methods for differential expression analysis of RNA-seq data. *BMC Bioinformatics* **14**, 91 (2013).
19. Maynard, K.R. et al. Transcriptome-scale spatial gene expression in the human dorsolateral prefrontal cortex. *Nature Neuroscience* **24**, 425-436 (2021).
20. Wang, M. et al. High-resolution 3D spatiotemporal transcriptomic maps of developing Drosophila embryos and larvae. *Developmental Cell* **57**, 1271-1283.e1274 (2022).
21. Ren, X., Wang, J., Liu, S. & Miecznikowski, J.C. (Department of Biostatistics, University at Buffalo.
22. Chandrasekaran, S. et al. Behavior-specific changes in transcriptional modules lead to distinct and predictable neurogenomic states. *Proceedings of the National Academy of Sciences* **108**, 18020-18025 (2011).

23. Shpigler, H.Y. et al. Deep evolutionary conservation of autism-related genes. *Proceedings of the National Academy of Sciences* **114**, 9653-9658 (2017).
24. Whitfield, C.W., Cziko, A.-M. & Robinson, G.E. Gene Expression Profiles in the Brain Predict Behavior in Individual Honey Bees. *Science* **302**, 296-299 (2003).
25. Avalos, A. et al. Genomic regions influencing aggressive behavior in honey bees are defined by colony allele frequencies. *Proceedings of the National Academy of Sciences* **117**, 17135-17141 (2020).
26. Traniello, I.M. et al. Single-cell dissection of aggression in honeybee colonies. *Nature Ecology & Evolution* **7**, 1232-1244 (2023).
27. Fahrbach, S.E. Structure of the mushroom bodies of the insect brain. *Annual review of entomology* **51**, 209-232 (2006).
28. Traniello, I.M., Chen, Z., Bagchi, V.A. & Robinson, G.E. Valence of social information is encoded in different subpopulations of mushroom body Kenyon cells in the honeybee brain. *Proc Biol Sci* **286**, 20190901 (2019).
29. Parker, R. et al. Correlation of proteome-wide changes with social immunity behaviors provides insight into resistance to the parasitic mite, Varroa destructor, in the honey bee (Apis mellifera). *Genome Biology* **13**, R81 (2012).
30. Moore, D. Honey bee circadian clocks: behavioral control from individual workers to whole-colony rhythms. *Journal of Insect Physiology* **47**, 843-857 (2001).
31. Moffitt, J.R. et al. Molecular, spatial, and functional single-cell profiling of the hypothalamic preoptic region. *Science* **362**, eaau5324 (2018).
32. Li, Z. & Zhou, X. BASS: multi-scale and multi-sample analysis enables accurate cell type clustering and spatial domain detection in spatial transcriptomic studies. *Genome Biology* **23**, 168 (2022).
33. Daubner, S.C., Le, T. & Wang, S. Tyrosine hydroxylase and regulation of dopamine synthesis. *Archives of Biochemistry and Biophysics* **508**, 1-12 (2011).
34. Morgenroth, V.H., Boadle-Biber, M. & Roth, R.H. Tyrosine Hydroxylase: Activation by Nerve Stimulation. *Proceedings of the National Academy of Sciences* **71**, 4283-4287 (1974).
35. Falkner, A.L. et al. Hierarchical Representations of Aggression in a Hypothalamic-Midbrain Circuit. *Neuron* **106**, 637-648.e636 (2020).
36. Daitz, H.M. & Powell, T.P.S. STUDIES OF THE CONNEXIONS OF THE FORNIX SYSTEM. *Journal of Neurology, Neurosurgery & Psychiatry* **17**, 75 (1954).
37. Haller, J., Makara, G.B. & Kruk, M.R. Catecholaminergic involvement in the control of aggression: hormones, the peripheral sympathetic, and central noradrenergic systems. *Neuroscience & Biobehavioral Reviews* **22**, 85-97 (1997).
38. He, Z.-X. et al. Substance P in the medial amygdala regulates aggressive behaviors in male mice. *Neuropsychopharmacology* **49**, 1689-1699 (2024).
39. Inada, K. et al. Plasticity of neural connections underlying oxytocin-mediated parental behaviors of male mice. *Neuron* **110**, 2009-2023.e2005 (2022).
40. Nakahara, T.S. et al. Peripheral oxytocin injection modulates vomeronasal sensory activity and reduces pup-directed aggression in male mice. *Scientific Reports* **10**, 19943 (2020).
41. Autry, A.E. et al. Urocortin-3 neurons in the mouse perifornical area promote infant-directed neglect and aggression. *eLife* **10**, e64680 (2021).
42. Wu, Z., Autry, A.E., Bergan, J.F., Watabe-Uchida, M. & Dulac, C.G. Galanin neurons in the medial preoptic area govern parental behaviour. *Nature* **509**, 325-330 (2014).
43. Tachikawa, K.S., Yoshihara, Y. & Kuroda, K.O. Behavioral Transition from Attack to Parenting in Male Mice: A Crucial Role of the Vomeronasal System. *The Journal of Neuroscience* **33**, 5120 (2013).
44. Grone, B.P. & Maruska, K.P. Three Distinct Glutamate Decarboxylase Genes in Vertebrates. *Scientific Reports* **6**, 30507 (2016).

45. Hao, S. et al. Cross-species single-cell spatial transcriptomic atlases of the cerebellar cortex. *Science* **385**, eado3927 (2024).
46. Vanrobaeys, Y. et al. Spatial transcriptomics reveals unique gene expression changes in different brain regions after sleep deprivation. *Nature Communications* **14**, 7095 (2023).
47. Ospina, O.E. et al. Differential gene expression analysis of spatial transcriptomic experiments using spatial mixed models. *Scientific Reports* **14**, 10967 (2024).
48. Qin, F., Luo, X., Cai, B., Xiao, F. & Cai, G. Spatial pattern and differential expression analysis with spatial transcriptomic data. *bioRxiv*, 2023.2007.2006.547967 (2023).
49. Mason, K. et al. Niche-DE: niche-differential gene expression analysis in spatial transcriptomics data identifies context-dependent cell-cell interactions. *Genome Biology* **25**, 14 (2024).
50. Wu, Z. et al. Graph deep learning for the characterization of tumour microenvironments from spatial protein profiles in tissue specimens. *Nature Biomedical Engineering* **6**, 1435-1448 (2022).
51. Liu, X., Zeira, R. & Raphael, B.J. PASTE2: Partial Alignment of Multi-slice Spatially Resolved Transcriptomics Data. *bioRxiv*, 2023.2001.2008.523162 (2023).
52. Clifton, K. et al. STalign: Alignment of spatial transcriptomics data using diffeomorphic metric mapping. *Nature Communications* **14**, 8123 (2023).
53. Kamada, T. & Kawai, S. An algorithm for drawing general undirected graphs. *Information Processing Letters* **31**, 7-15 (1989).
54. Wang, G., Moffitt, J.R. & Zhuang, X. Multiplexed imaging of high-density libraries of RNAs with MERFISH and expansion microscopy. *Scientific Reports* **8**, 4847 (2018).
55. Emanuel, G., Eichhorn, S.W. & Zhuang, X., Vol. 0.1.6 (Zenodo, 2020).
56. Stringer, C., Wang, T., Michaelos, M. & Pachitariu, M. Cellpose: a generalist algorithm for cellular segmentation. *Nature Methods* **18**, 100-106 (2021).

Figure Legends

Figure 1. Overview of SpaceExpress Framework and Evaluations of SpaceExpress cell embeddings on synthetic data.

(A) SpaceExpress detects differential spatial expression between two tissue samples. In its first step (bottom), SpaceExpress maps ("embeds") cells of each tissue sample in a common latent space based on their locations as well as gene expression profiles. Dimensions of the learnt latent space define an intrinsic coordinate system shared by the samples, assigning similar coordinates to analogous tissue structures. In step 2 (top), each gene G is analyzed for differential spatial expression (DSE) between the tissue samples: spline regression is used to model the gene's expression in a cell as a function of the cell's coordinate along a particular dimension, and a statistical test is performed to assess whether this function differs between the samples, with the results quantified as a false discovery rate (FDR). (This is repeated for each dimension.) The same approach also applies to detecting a gene's DSE between two groups of samples. (**B)** Schematic of step 1 of SpaceExpress. Spatial information in given tissue sample(s) is represented by a nearest neighbor graph of cells, with distances between cells (e.g., d_{ij} between cells i and j) defined as shortest path lengths between them and reflecting their physical proximity in the tissue. Expression profile of each cell (g_i) is mapped by an encoder (neural network) to a low-dimensional embedding, so that Euclidean distances between cells in the embedding space (e.g., $|p_i - p_j|$) approximate their spatial distances (e.g., d_{ij}). For simplicity, three dimensions are shown in the embedding space. (**C)** Synthetic "early embryo" data set comprises cells arranged in an elliptical idealized embryo, with expression data on 100 genes whose spatial expression distribution has an anterior-posterior (AP) pattern, a dorsal-ventral (DV) pattern, a combination of AP and DV patterns (APDV) or a random distribution. In total, 10 replicates with different random noise were generated. **(D)** Schematic of Jaccard Similarity (JS) measure for evaluating SpaceExpress cell embeddings. Two neighborhood networks are constructed: the x-knn network, based on physical cell locations (x, y), and the p-knn network, based on the cell embeddings (panel B). JS (size of intersection divided by size of union) of the edges in these two networks is then used to quantify the similarity between these networks, providing a measure of how well the embedding preserves spatial relationships. JS has maximum value (1) when the two graphs are identical and its minimum value (0) if the two graphs share no edges. **(E)** Box plots of JS scores on synthetic early embryo data sets (n=10 replicates), comparing the performance of different embedding methods—SEDR, GraphST, STAGATE, and SpaceExpress. Higher JS scores indicate a better preservation of spatial structure in the embedding. **(F)** PCA visualizations of cell embeddings generated by SEDR, GraphST, STAGATE, and SpaceExpress for a synthetic early embryo data set. Each point represents a cell, colored by its position along the anterior-posterior (AP) axis. **(G)** Visualization of two of the embedding dimensions learnt by SpaceExpress from the synthetic early embryo data. Each point represents a cell at its physical location, colored by its coordinate value in the respective embedding dimension. **(H)** Illustration of the spatial regions within the synthetic "domain grid" data set. Nine square regions, each comprising 10 x 10 cells (are arranged in a 3 x 3 grid representing the tissue sample. Each region (shown in a different color) is marked by exclusive expression of one gene, while 91 additional genes are assigned random expression values. **(I)** Box plot of JS scores on synthetic "domain grid" data sets (n=10 replicates) for the four methods (SEDR, GraphST, STAGATE, and SpaceExpress**). (J)** PCA

visualizations of spatial embeddings across methods, with points colored by their spatial regions (panel F) in the synthetic tissue.

Figure 2. Evaluations of SpaceExpress cell embeddings on real data. (A) Box plots showing Jaccard Similarity (JS) scores on 12 tissue samples from the DLPFC dataset when embedding cells in a tissue using SEDR, GraphST, STAGATE, or SpaceExpress. (**B, C)** Visualization of tissue samples ID 151507 (B) and ID 151672 (C), showing spatial tissue organization into cortex layers and white matter (left panel) and a colormap visualization of one of the embedding dimensions learnt by SpaceExpress (right panel). (**D)** PCA plots of cell embeddings learnt by different methods on tissue sample ID 151507. Points are colored according to their cortex layer assignments (panel B). (**E)** Box plot of JS scores on 16 slices of Drosophila embryo (E14-16) data, comparing the performance of the four embedding methods. (**F)** Visualization of Drosophila embryo slice S08, with colors indicating annotated spatial regions/tissues. (**G)** PCA plots of SpaceExpress cell embeddings of Drosophila embryo slice S08, showing that the learnt embeddings capture known tissue structure.

Figure 3. SpaceExpress embeddings capture a universal coordinate system. (A) SpaceExpress cell embedding function trained on one DLPFC sample (ID 151507, Figure 2B) was used to embed (assign coordinates to) cells in a different sample (ID 151676), using only expression (without spatial) data from the latter. Distances between embeddings of cell pairs (y axis) were compared to their physical distance (Euclidean distance) (x axis), for cell pairs belong to the different layers (left) or same layer (right) of the tissue. Each point in the inter-layer plot (left) represents one pair of layers, showing the (physical or embedding) distances between centroids of the two layers**.** The intra-layer plot (right) is a 2D histogram of the joint distribution of embedding and physical distances between cell pairs in the same layer, aggregated over all layers. **(B)** Evaluation of a cell mapping method, Tangram, using the same procedure as in (A). **(C, D)** Visualization of Drosophila embryo slices S06 (C) and S07 (D), where cells are colored based on their annotated spatial regions/tissues. **(E)** Box plot of Jaccard Similarity (JS) values of SpaceExpress embeddings for slices S06 and S07, obtained without using spatial information on these tissues. Also shown for comparison are corresponding JS scores of a random baseline ("Permuted") where SpaceExpress embeddings were trained on a version of slices S08 where the spatial locations of cells were randomly permuted. **(F)** Example of a gene whose spatial expression pattern differs between two synthetic early embryos. The gene is an "APDV" gene (Figure 1C), i.e., a gene with anterior-posterior (AP) as well as dorso-ventral (DV) expression pattern, with a parameter μ denoting the weight of the AP pattern. In this example, μ is set to 0 and 0.6 in the two embryos, resulting in a purely DV pattern in the former case (left) and a mix of AP and DV patterns in the latter case (right). **(G)** SpaceExpress embedding values (dimension 1) of cells in the two synthetic early embryos from (F), showing that this dimension captures the AP axis of both embryos. **(H)** Embedding values of "corresponding" cells in the two synthetic embryos, including all four dimensions. By design there is a one-one correspondence between cells of the two embryos, with each corresponding pair agreeing in spatial location and 80% of transcriptome. The high correlation shows that SpaceExpress learns shared dimensions. **(I)** Expression value of the gene shown in (F), in cells of both synthetic embryos (yellow and green), plotted against the cell's embedding value in dimension 1. Curves represent spline model fits, and

reveal that gene expression distribution along the embedding dimension differs between two samples.

Figure 4. **SpaceExpress identifies differential spatial expression of genes in honey bee brain. (A)** Transcriptome map for forager and soldier honey bee brains. Each spot represents a transcript (n= 11,373 and 10,334 respectively) with color representing gene identity. **(B)** Visualization of SpaceExpress cell embeddings for the two honey bee brain samples, in all four dimensions. Each point corresponds to an individual cell at its spatial location, colored by the embedding value for each dimension. **(C)** Venn diagram showing the overlaps among sets of gene exhibiting Differential Spatial Expression (DSE) in each of the four embedding dimensions (Dim 1-4). (**D, F, H**) Spatial expression visualization of select DSE genes. The expression levels of *hr38* (D), *fasciclin-1* (F), and *per* (H), are shown. Cells with higher expression levels of each gene are colored in darker shades of red, revealing distinct patterns of spatial expression in different brain regions. **(E, G, I)** Gene expression versus embedding dimension plots. These plots display spline model fits for gene expression levels of *hr38* (E), *fasciclin-1* (G), and *per* (I) against the embedding dimension in which DSE was detected as significant. See text for how to interpret DSE based on gene-specific visualizations (D-I) and embedding dimension visualizations (B).

Figure 5. SpaceExpress identifies differential spatial expression of genes in mouse hypothalamic preoptic **region related to pup-directed aggression. (A)** Neuroanatomical annotation of cells in the hypothalamic preoptic region for naïve and a pup-exposed aggressive mouse, obtained computationally by mapping the cells to a reference tissue sample with manual annotations (Methods). Cells are color-coded according to their respective regional annotations, including the third ventricle (V3), bed nuclei of the strata terminalis (BST), columns of the fornix (fx), medial preoptic area (MPA), medial preoptic nucleus (MPN), periventricular hypothalamic nucleus (PV), paraventricular hypothalamic nucleus (PVH), and paraventricular nucleus of the thalamus (PVT). **(B)** Venn diagram illustrating the overlaps among sets of DSE genes across the four embedding dimensions (Dim 1 to 4) **(C)** SpaceExpress embeddings visualized across four dimensions for both the naïve and pup-exposed mouse brains. Each cell is represented by a point, positioned according to its spatial location and colored by the corresponding embedding value for each dimension. The arrows highlight specific regions that correspond to the same areas shown in Figure 5A, with matching colors representing the same anatomical regions. (**D, E**) Spatial expression visualization and gene expression versus embedding dimension plots for select genes. Shown are the expression levels (grey-red colormaps) of *Th* (C) and *Slc17a6* (D) in both naïve and pup-exposed samples, alongside spline model fits for gene expression along the respective embedding dimensions where significant DSE was detected.

Figure 6. SpaceExpress identifies genes with differential spatial expression between two groups with multiple biological replicates. Shown are spatial expression (grey-red colormaps) and embedding dimension (full spectrum colormaps) visualizations for *Oxt* (A) and *Gad1* (B) in whole brain of naïve and pup-exposed mice. The six columns represent three replicates from the

naïve group and three from the pup-exposed group. The plots on the right show spline model fits of gene expression against coordinate values for the embedding dimension visualized.

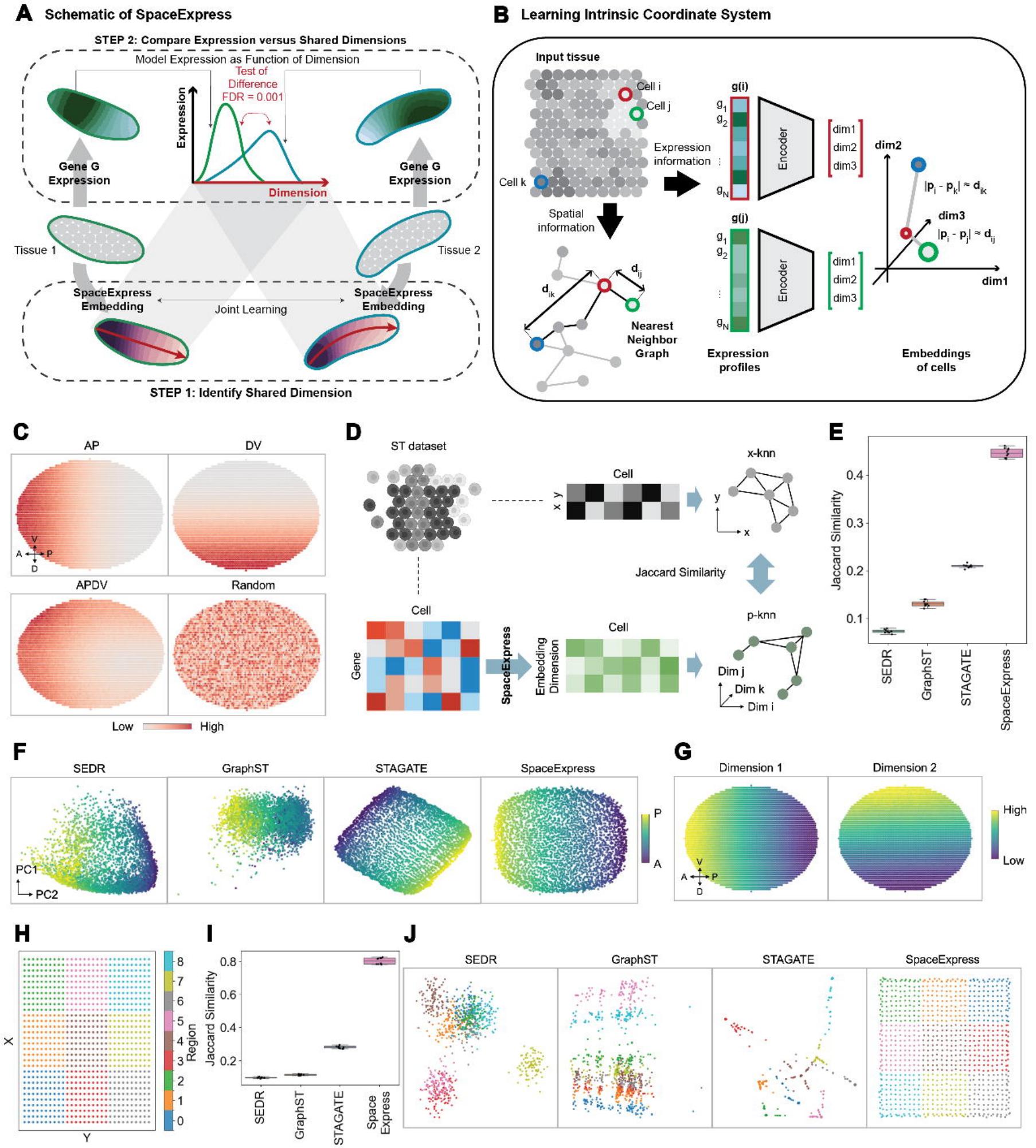
A
Schematic of SpaceExpress
STEP 2: Compare Expression versus Shared Dimensions
Model Expression as Function of Dimension
Test of Difference FDR = 0.001
Expression
Dimension
Gene G Expression
Gene G Expression
Tissue 1
Tissue 2
SpaceExpress Embedding
Joint Learning
SpaceExpress Embedding
STEP 1: Identify Shared Dimension
B
Learning Intrinsic Coordinate System
Input tissue
Cell i
Cell j
Cell k
Expression information
Spatial information
g(i)
g(j)
Encoder
Encoder
dim1
dim2
dim3
Nearest Neighbor Graph
Expression profiles
Embeddings of cells
C
AP
DV
APDV
Random
Low
High
D
ST dataset
Cell
Gene
SpaceExpress
Embedding Dimension
x-knn
p-knn
Jaccard Similarity
E
Jaccard Similarity
SEDR
GraphST
STAGATE
SpaceExpress
F
SEDR
GraphST
STAGATE
SpaceExpress
PC1
PC2
P
A
G
Dimension 1
Dimension 2
High
Low
H
Region
X
Y
I
Jaccard Similarity
SEDR
GraphST
STAGATE
Space Express
J
SEDR
GraphST
STAGATE
SpaceExpress

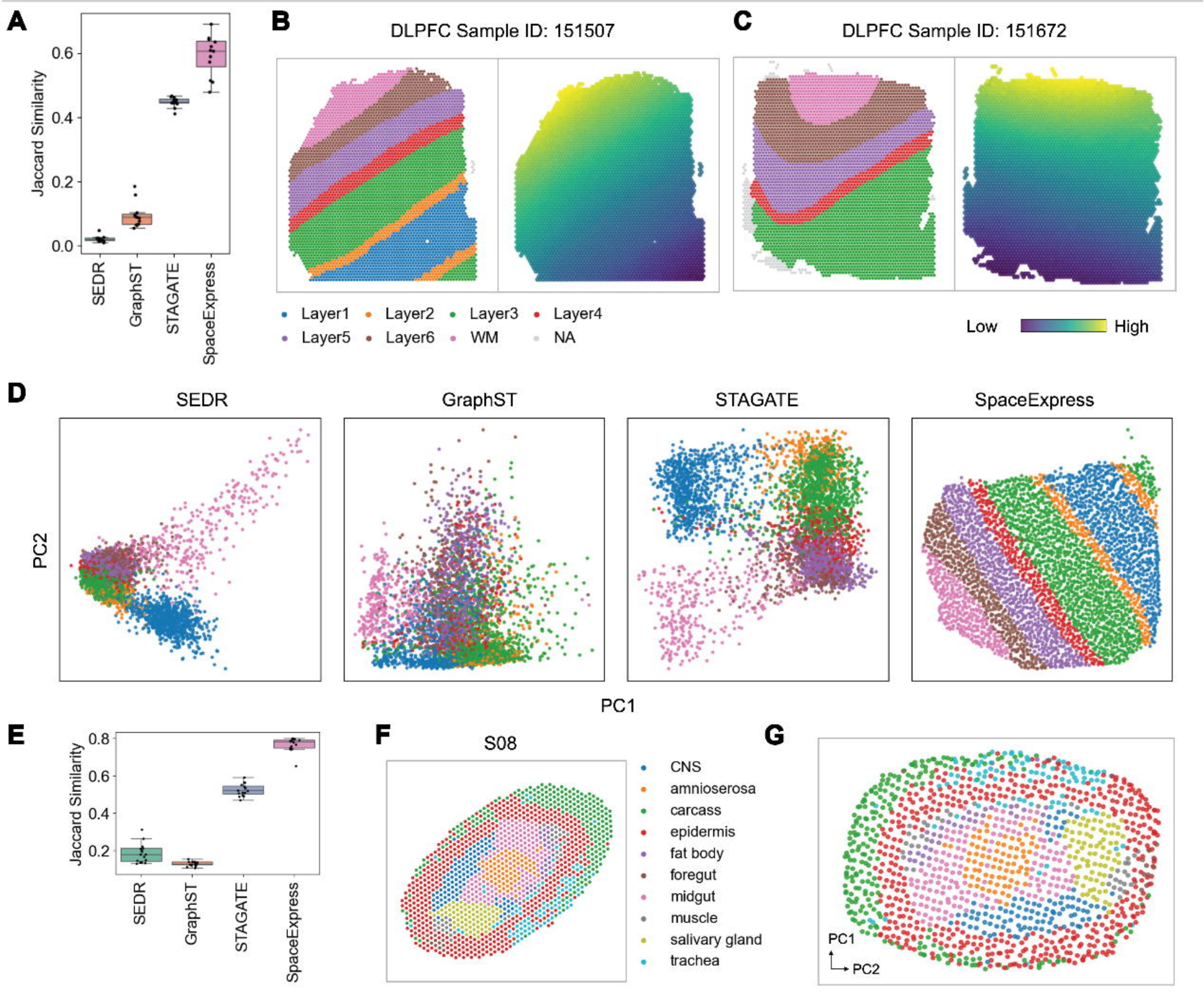
A
Jaccard Similarity
0.0
0.2
0.4
0.6
SEDR
GraphST
STAGATE
SpaceExpress
B
DLPFC Sample ID: 151507
Layer1
Layer2
Layer3
Layer4
Layer5
Layer6
WM
NA
C
DLPFC Sample ID: 151672
Low
High
D
SEDR
GraphST
STAGATE
SpaceExpress
PC2
PC1
E
Jaccard Similarity
0.2
0.4
0.6
0.8
SEDR
GraphST
STAGATE
SpaceExpress
F
S08
CNS
amnioserosa
carcass
epidermis
fat body
foregut
midgut
muscle
salivary gland
trachea
G
PC1
PC2

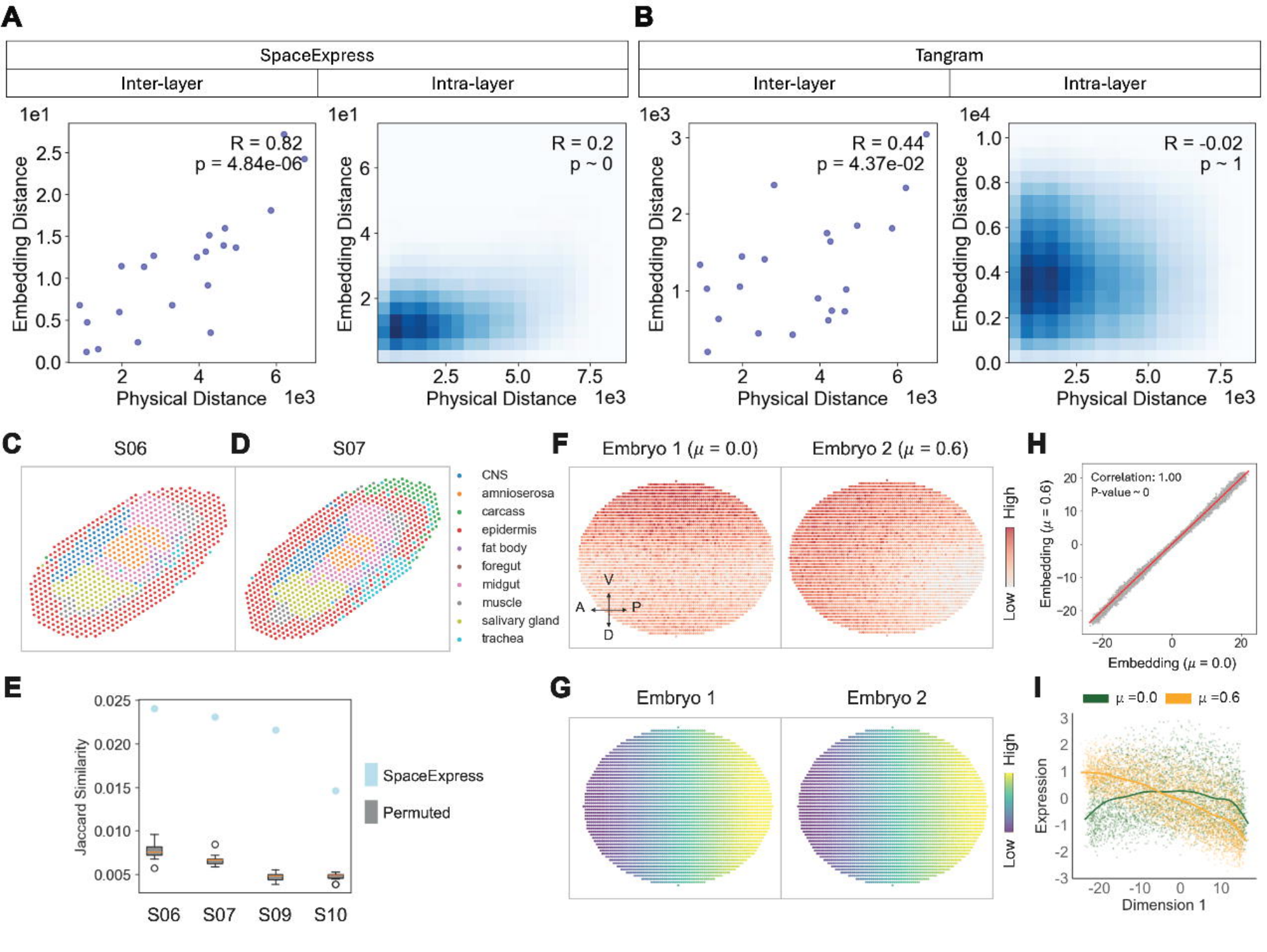
A
SpaceExpress
Inter-layer
Intra-layer
R = 0.82
p = 4.84e-06
R = 0.2
p ~ 0
Embedding Distance
Physical Distance
1e1
1e3
B
Tangram
Inter-layer
Intra-layer
R = 0.44
p = 4.37e-02
R = -0.02
p ~ 1
1e4
C
S06
D
S07
CNS
amnioserosa
carcass
epidermis
fat body
foregut
midgut
muscle
salivary gland
trachea
F
Embryo 1 (μ = 0.0)
Embryo 2 (μ = 0.6)
V
A
P
D
High
Low
H
Correlation: 1.00
P-value ~ 0
Embedding (μ = 0.6)
Embedding (μ = 0.0)
E
Jaccard Similarity
SpaceExpress
Permuted
S06
S07
S09
S10
G
Embryo 1
Embryo 2
High
Low
I
μ =0.0
μ =0.6
Expression
Dimension 1

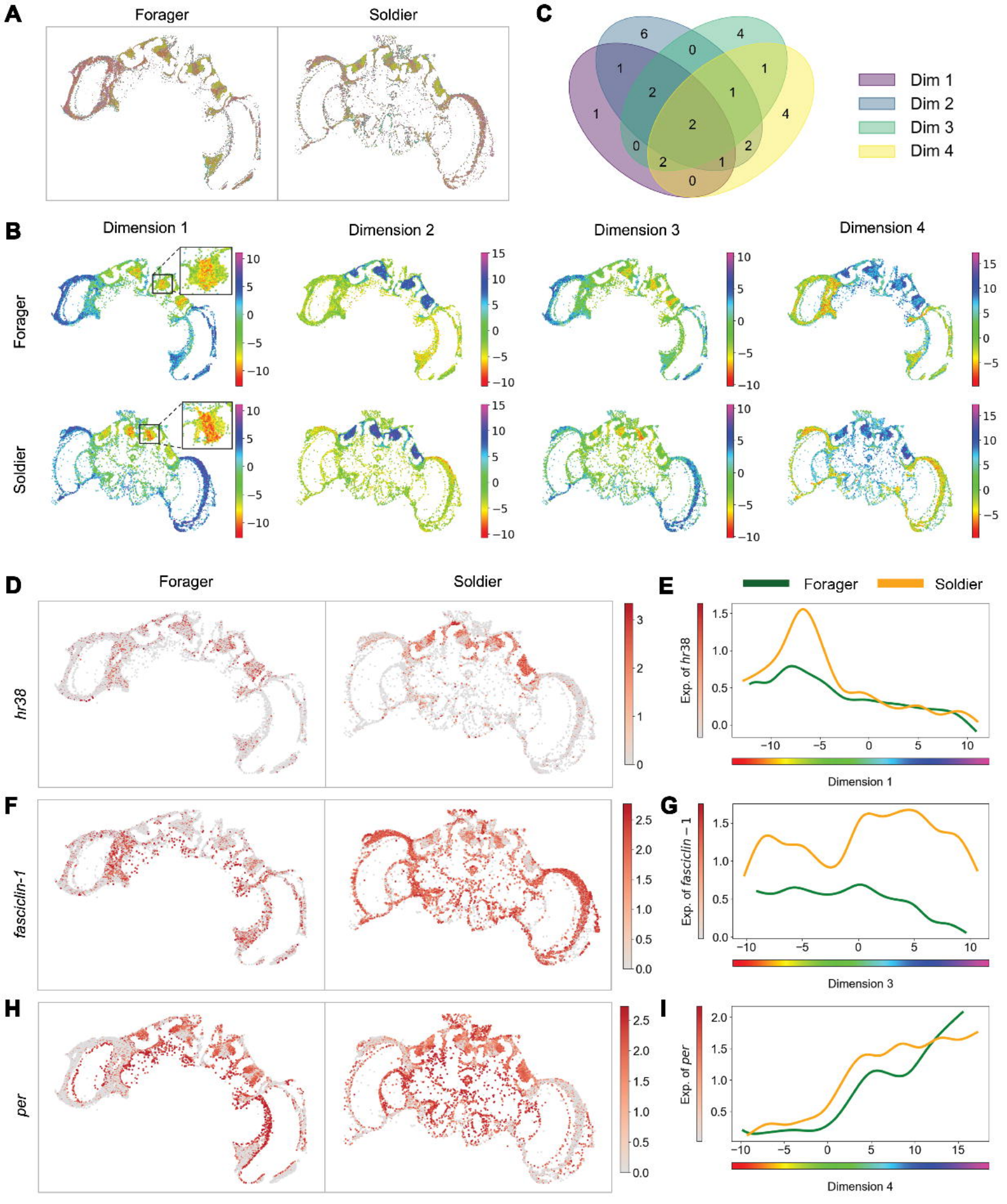
A
Forager
Soldier
C
Dim 1
Dim 2
Dim 3
Dim 4
B
Dimension 1
Dimension 2
Dimension 3
Dimension 4
Forager
Soldier
D
Forager
Soldier
hr38
E
Forager
Soldier
Exp. of hr38
Dimension 1
F
fasciclin-1
G
Exp. of fasciclin − 1
Dimension 3
H
per
I
Exp. of per
Dimension 4

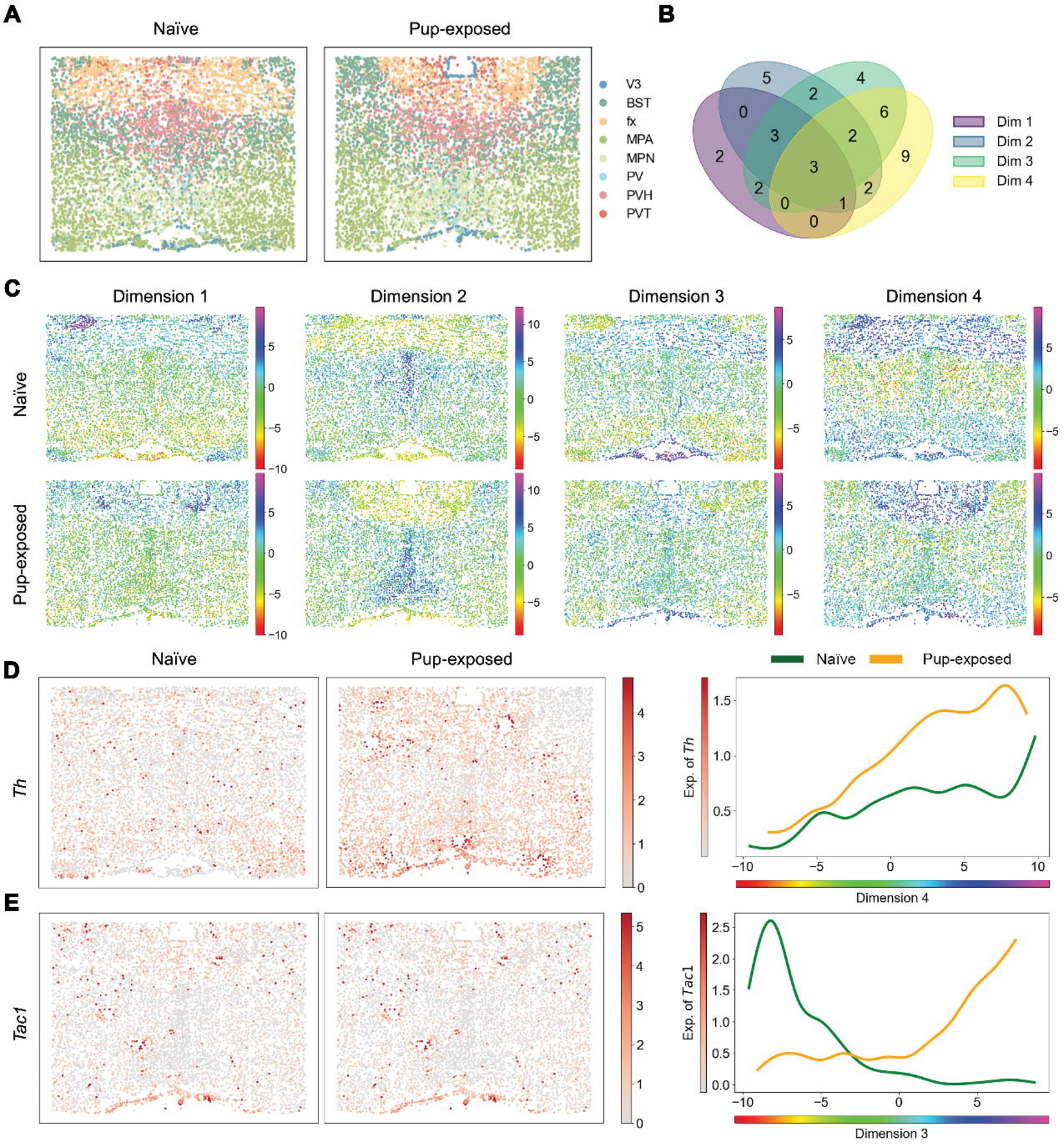
A
Naïve
Pup-exposed
V3
BST
fx
MPA
MPN
PV
PVH
PVT
B
Dim 1
Dim 2
Dim 3
Dim 4
C
Dimension 1
Dimension 2
Dimension 3
Dimension 4
Naïve
Pup-exposed
D
Th
Naïve
Pup-exposed
Exp. of Th
Dimension 4
E
Tac1
Exp. of Tac1
Dimension 3

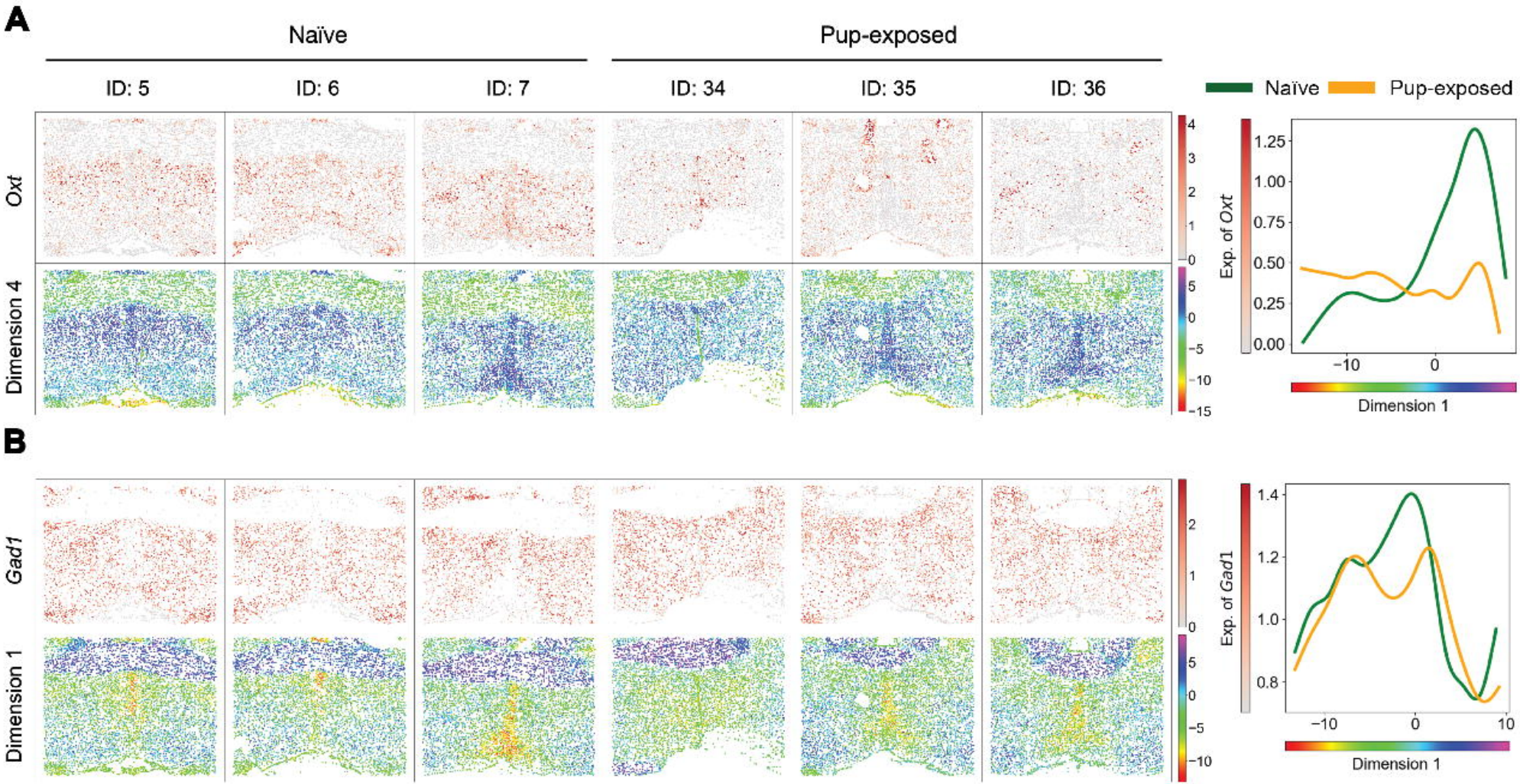
A
Naïve
Pup-exposed
ID: 5
ID: 6
ID: 7
ID: 34
ID: 35
ID: 36
Naïve
Pup-exposed
Oxt
Dimension 4
Exp. of Oxt
Dimension 1
B
Gad1
Dimension 1
Exp. of Gad1
Dimension 1